The Quantum Zeno Effect as Suppression of Irreversible Commitment: A Quantitative Analysis in Continuously Measured Superconducting Qubits

Keith Taylor *VERSF Theoretical Physics Program*

Plain Language Summary

If you watch a quantum system closely enough, it stops changing. This is the Quantum Zeno Effect — named after the ancient Greek philosopher who argued that an arrow in flight is, at any instant, motionless. In quantum physics, the equivalent claim is that sufficiently frequent observation can freeze a system in place, preventing it from transitioning from one state to another. The effect is real, has been measured in laboratory experiments with superconducting quantum bits, and is quantitatively well understood.

What is *not* settled is why it happens. The standard explanation says that measurement destroys the quantum coherence — the subtle interference between possibilities — that drives transitions. Without coherence, the system cannot evolve. This paper proposes a different account: measurement does not primarily destroy coherence. Instead, it prevents the system from reaching the point at which a definite outcome becomes physically irreversible.

The distinction matters. In the standard view, coherence and outcome-formation are part of the same process — break one and you break both. In the framework developed here (the Void Energy-Regulated Space Framework, or VERSF), these are two separate stages. A system can lose coherence without yet having committed to an outcome, and it is the commitment stage — not coherence alone — that measurement is interrupting.

This is not merely a philosophical reinterpretation. The two accounts make different mathematical predictions in three specific experimental regimes: when the driving force is very strong, when measurement is very weak, and near the boundary where measurement starts accelerating transitions rather than suppressing them. The paper derives those differences precisely, shows they are measurable with existing technology, and explains exactly what experimental result would prove the standard account right and the VERSF account wrong.

Table of Contents

Abstract

The Quantum Zeno Effect (QZE) is standardly interpreted as suppression of coherent quantum evolution by frequent measurement, mediated through measurement-induced dephasing. In continuously measured superconducting qubit systems, this suppression is quantitatively described by the driven transition rate $\Gamma\uparrow = \Omega^2/[2(\gamma_2 + \Gamma\_d)]$, validated across a broad parameter range in circuit quantum electrodynamics. We present a reanalysis of this formula within the Void Energy-Regulated Space Framework (VERSF), in which irreversible physical outcomes are constituted only upon crossing a structural commitment threshold $B\_R \geq C\_R$. We introduce explicit linear dynamics for the distinguishability accumulation variable $B\_R(t)$ driven by coherent amplitude and interrupted by measurement interactions, and show that these dynamics reproduce the standard QZE formula exactly at leading order. At higher drive strengths and in weak-measurement regimes, the VERSF dynamics generate corrections distinct from those arising in decoherence-only accounts. Specifically, we derive that the VERSF predicts an additional suppression term of order $(\Omega/\Gamma\_m)^2$ at high drive, and predicts that the Anti-Zeno transition threshold depends on the embedding coefficient η of the measurement interaction rather than on its spectral density alone. We identify three experimentally accessible regimes—high-drive deviation, non-exponential weak-measurement decay, and Anti-Zeno threshold structure—in which the two interpretations yield quantitatively distinct predictions, and propose concrete protocols for discriminating them.

---

1. Introduction

The Quantum Zeno Effect (QZE), first formalized by Misra and Sudarshan [1], describes the inhibition of quantum transitions under sufficiently frequent observation. In its continuous-measurement formulation, applicable to superconducting qubit platforms [2,3], the effect is parameterized by a measurement-induced dephasing rate Γ_d that suppresses driven transitions in proportion to measurement strength. This formulation has been quantitatively validated in circuit quantum electrodynamics (cQED) experiments achieving simultaneous control of drive amplitude, measurement rate, and intrinsic decoherence [4,5].

Despite its mathematical precision, the physical interpretation of the QZE remains genuinely open. The standard account attributes transition suppression to the destruction of coherence: measurement collapses off-diagonal density matrix elements, preventing phase accumulation necessary for transition. This is a dynamical account in which coherence and outcome-formation are treated as aspects of a single process.

The Void Energy-Regulated Space Framework (VERSF) distinguishes these processes structurally. In VERSF, coherent dynamical evolution and the formation of irreversible outcomes are separated by a commitment threshold: an outcome becomes a fact only when the accumulated distinguishability cost B_R reaches the local structural capacity C_R. Prior to threshold crossing, the system evolves but has not yet committed. The QZE, on this account, operates not by destroying coherence but by suppressing the accumulation of distinguishability

required to reach irreversible commitment — repeatedly interrupting B_R before any single trajectory can cross the threshold.

This interpretive distinction is physically meaningful only if it implies different predictions in some regime. In this paper we derive those predictions explicitly. We show that the standard QZE formula is recovered as the leading-order limit of VERSF commitment dynamics, identify the corrections that emerge at higher order, and propose experimental tests capable of discriminating the two accounts.

To orient the reader: in standard terms, measurement suppresses coherent evolution by destroying off-diagonal density matrix elements. In VERSF terms, it prevents the system from reaching the point at which an outcome becomes irreversible. These are mathematically equivalent at leading order — which is why all existing QZE data are consistent with both accounts — but they differ in how and where deviations arise. The goal of this paper is to identify those deviations precisely.

The paper is organized as follows. Section 2 reviews the standard QZE formalism in continuously measured qubits. Section 3 introduces the VERSF commitment dynamics for B_R(t) with explicit parameter definitions. Section 4 demonstrates leading-order equivalence and derives higher-order VERSF corrections. Section 5 presents a systematic numerical evaluation across the experimentally reported parameter range. Section 6 analyzes the three divergence regimes. Section 7 develops concrete testable predictions and experimental protocols. Section 8 discusses the implications and limitations. Section 9 concludes.

---

2. Standard QZE Formalism in Continuously Measured Qubits

Consider a driven two-level system (qubit) subject to continuous homodyne measurement. The Lindblad master equation for the qubit density matrix ρ is:

$\dot{\rho} = -i[H_{drive}, \rho] + \gamma_2 \mathcal{D}[\sigma_z]\rho + \Gamma_d \mathcal{D}[\sigma_z]\rho$

where $H_{drive} = (\Omega/2)\sigma_x$, γ_2 is the intrinsic pure dephasing rate, Γ_d is the measurement-induced dephasing rate, and $\mathcal{D}[A]\rho = A\rho A^\dagger - (1/2)\{A^\dagger A, \rho\}$.

The steady-state driven transition rate, derived in the secular approximation valid for $\Omega \ll (\gamma_2 + \Gamma_d)$, is [4,6]:

$\Gamma_\uparrow = \Omega^2 / [2(\gamma_2 + \Gamma_d)]$ (1)

Using the standard relation between measurement rate Γ_m and dephasing $\Gamma_d = \Gamma_m/2$ [3]:

$\Gamma_\uparrow = \Omega^2 / (\Gamma_m + 2\gamma_2)$ (2)

In the Zeno regime $\Gamma_m \gg \gamma_2$, equation (2) reduces to:

$$\Gamma\uparrow^{Zeno} \approx (\Omega^2/\Gamma_m)\,[1 - 2\gamma_2/\Gamma_m + \mathcal{O}(\gamma_2/\Gamma_m)^2] \quad (3)$$

The leading term Ω^2/Γ_m is the signature of the QZE: transition rate falls as measurement strength increases. The correction term $2\gamma_2/\Gamma_m$ remains small throughout the strong-measurement regime.

The Anti-Zeno Effect (AZE) — measurement-enhanced rather than suppressed transitions — occurs when the effective spectral density of the measurement process overlaps with the qubit transition frequency ω_0. In the standard account, the AZE/Zeno boundary occurs at a critical measurement rate Γ_m^* determined by the environmental spectral function $J(\omega)$ [7]:

$$\Gamma_m^* = \arg\min_{\Gamma_m}\,[\Gamma\uparrow(\Gamma_m)] \approx \sqrt{(J(\omega_0)\cdot\omega_0)} \quad (4)$$

This spectral-function dependence is a specific and testable prediction of the standard account.

---

3. VERSF Commitment Dynamics

3.1 Fundamental Postulates

In VERSF, each local region R of spacetime is characterized by two quantities:

- **$B_R(t)$**: The accumulated distinguishability cost — a non-negative scalar measuring the integrated structural departure from the zero-entropy void substrate.
- **C_R**: The local structural capacity — a finite threshold above which the region cannot absorb further distinguishability without committing an irreversible outcome.

An irreversible physical outcome (a "fact") is formed if and only if:

$$B_R(t) \geq C_R \quad (5)$$

Prior to threshold crossing, the system evolves within the commitment lag — a finite interval during which quantum amplitudes remain physically meaningful but no definite outcome has been established.

3.2 Justification of the B_R Dynamics

Equation (6) below is not derived from first principles in the present paper — a full derivation from the VERSF substrate equations is reserved for subsequent work. However, its functional form is uniquely constrained by four requirements that any acceptable dynamics must satisfy:

(i) Monotonic accumulation under coherent drive. In the absence of measurement ($\Gamma_m = 0$, $\kappa = 0$), B_R must increase under coherent drive. The drive contribution must be non-negative and proportional to Ω^2 rather than Ω, because B_R accumulates from squared amplitude — analogous to how energy density depends on field amplitude squared, and how distinguishability in quantum information scales with the square of state overlap differences.

(ii) Linear resetting under measurement. Each measurement interaction interrupts the accumulated trajectory. In the Markovian limit — valid when measurement correlation times are short compared to B_R accumulation times — the interruption acts as a linear drain proportional to current B_R and to measurement rate Γ_m. A nonlinear interruption term (e.g., $\Gamma_m B_R^2$) would not recover the standard QZE formula at leading order, violating consistency with established experiment.

(iii) Saturation under finite capacity. Since C_R is finite, accumulation must slow as B_R approaches C_R. The minimal term encoding this is $-\kappa B_R^2$, which generates a finite fixed point below C_R at high drive. Higher-order terms are suppressed by additional powers of B_R/C_R and are negligible in the regimes considered.

(iv) Dimensional consistency. With $[B_R]$ chosen to have dimensions of $[\mu s^{-1}]$ (matching the natural scale of transition rates), $[\eta]$ dimensionless, $[\Omega^2]$ in $[\mu s^{-2}]$, $[\Gamma_m]$ in $[\mu s^{-1}]$, and $[\kappa]$ in $[\mu s]$, equation (6) is dimensionally consistent throughout.

Equation (6) is therefore the minimal admissible form satisfying all four constraints simultaneously. We do not claim uniqueness: a measurement term of the form $\Gamma_m(B_R + \varepsilon B_R^2)$, for example, would also satisfy constraints (i)–(iv) at leading order. However, such alternatives introduce additional free parameters while recovering identical leading-order predictions. Equation (6) is the minimal expression in the sense that it contains the fewest terms consistent with all four requirements, and any alternative satisfying the same constraints will coincide with equation (6) at the order of approximation used in this paper.

3.3 Dynamics of B_R

We model the evolution of B_R under coherent drive and measurement interaction as:

$$dB_R/dt = \eta\Omega^2 - \Gamma_m B_R - \kappa B_R^2 \quad (6)$$

where:

- **Ω^2** is the squared drive amplitude, which drives distinguishability accumulation;
- **Γ_m** is the measurement rate, which interrupts B_R accumulation — each measurement interaction resets the accumulated trajectory through projection or confirmation of the system state, acting as a linear drain on B_R proportional to Γ_m;
- **η** is the **embedding coefficient** — a dimensionless parameter $\in (0, \infty)$ quantifying the efficiency with which coherent amplitude contributes to distinguishability accumulation, determined by the geometric and dynamical coupling between the driven system and its local region R. $\eta = 1$ corresponds to ideal coupling; $\eta > 1$ occurs when the measurement

interaction itself contributes to B_R accumulation (the regime underlying the Anti-Zeno Effect, where measurement tone and qubit transition frequency are near-resonant); $\eta < 1$ reflects partial structural decoupling. Because η depends on coupling geometry and detuning — quantities independently controllable in cQED — it is in principle measurable;

- **κ** is the **nonlinear saturation coefficient** (dimensions: [μs]) representing the increasing cost of additional distinguishability contributions as B_R approaches C_R: as the local region nears its structural capacity, each additional unit of drive contributes less to B_R accumulation. This is the dynamical expression of the finite capacity C_R — saturation is not an ad hoc term but the direct consequence of C_R being finite. The effect is negligible at low Ω and becomes significant only when $B_R^{(\infty)}$ is an appreciable fraction of C_R.

3.4 Fixed Points and Threshold Crossing Rate

Setting $\kappa = 0$ for the linear regime, the fixed point of equation (6) is:

$$B_R^{(\infty)} = \eta\Omega^2/\Gamma_m \quad (7)$$

The system relaxes toward $B_R^{(\infty)}$ with characteristic time $\tau_B = 1/\Gamma_m$. A transition occurs when B_R reaches C_R, which happens if and only if $B_R^{(\infty)} \geq C_R$, i.e.:

$$\eta\Omega^2/\Gamma_m \geq C_R \quad (8)$$

We treat threshold crossing as a first-passage process under stochastic measurement back-action, consistent with quantum trajectory descriptions [6]. Under continuous homodyne measurement, measurement back-action generates a diffusion term in B_R; the full stochastic equation is:

$$dB_R = (\eta\Omega^2 - \Gamma_m B_R - \kappa B_R^2)dt + \sigma\sqrt{\Gamma_m}\, dW_t \quad (9)$$

where dW_t is a Wiener increment and σ is the measurement back-action strength, set by the homodyne detection efficiency $\eta_{det} \in (0, 1]$ via $\sigma^2 = 1 - \eta_{det}$ in the standard quantum trajectory formalism [3]; σ is therefore independently measurable through homodyne efficiency calibration. The diffusion coefficient in the B_R equation inherits this relation through the same coupling η that governs drive-amplitude accumulation: the measurement back-action noise on B_R is taken proportional to the measurement back-action noise on the physical trajectory, scaled by η. Equation (9) has the form of a drift-diffusion equation well known in stochastic process theory [see, e.g., Gardiner, *Handbook of Stochastic Methods*, 4th ed.], with drift toward the fixed point $B_R^{(\infty)}$ and diffusion setting the width of the threshold-crossing time distribution. In the strong-measurement limit, the drift term dominates and individual trajectories diffuse stochastically toward or away from C_R under the combined influence of coherent drive and measurement-induced noise. A full derivation of the mean first-passage time from the associated Fokker-Planck equation is reserved for subsequent work. In the drift-dominated strong-measurement regime, the leading-order approximation gives:

$$\Gamma\uparrow^{VERSF} = 1/T_{FP} \approx \eta\Omega^2/(C_R\, \Gamma_m) \quad (10)$$

at leading order in the strong-measurement regime.

---

4. Leading-Order Equivalence and Higher-Order Divergence

4.1 Recovering the Standard Formula

Equation (10) reproduces the standard Zeno scaling Ω^2/Γ_m, with the ratio η/C_R acting as an effective proportionality constant setting the scale of this dependence in the strong-measurement regime. The correspondence with equation (3) requires $\eta/C_R = 1$, which is a calibration condition: since both η and C_R are free parameters of VERSF at this stage, this identification fixes one parameter combination rather than constituting a parameter-free derivation. This is legitimate and standard practice when introducing a new dynamical variable, but it should be stated transparently. In the limit $\Gamma_m \gg \gamma_2$ with η/C_R calibrated to unity, equation (10) is in full quantitative agreement with equation (3). The two frameworks are therefore empirically indistinguishable at leading order in Ω/Γ_m and γ_2/Γ_m. This is not a weakness: it confirms that VERSF is consistent with all existing QZE measurements, while making the interpretation of the Γ_m^{-1} scaling physically distinct.

4.2 Higher-Order Corrections from Nonlinear Dynamics

Retaining the κ term in equation (6), the fixed point becomes:

$$B_R^{(\infty)} = (\Gamma_m/2\kappa)[\sqrt{(1 + 4\eta\kappa\Omega^2/\Gamma_m^2)} - 1] \approx \eta\Omega^2/\Gamma_m - \eta^2\kappa\Omega^4/\Gamma_m^3 + \mathcal{O}(\Omega^6/\Gamma_m^5) \quad (11)$$

The first-passage rate then acquires a negative correction at high drive:

$$\Gamma\uparrow^{VERSF} \approx (\eta\Omega^2/C_R\,\Gamma_m)\,[1 - \eta\kappa\Omega^2/\Gamma_m^2] \quad (12)$$

This predicts that in the high-drive regime, the observed transition rate will fall *below* the leading-order Zeno prediction, with a correction scaling as $(\Omega/\Gamma_m)^2$. The standard framework attributes high-drive deviations to higher-order terms in the secular approximation used to derive equation (1); these corrections scale differently (as Ω/γ_2 rather than Ω/Γ_m). The power-law structure of the deviation therefore provides a discriminating signature. Figure 1 illustrates this divergence: the two predictions are indistinguishable within the current experimental range and separate clearly at higher drive.

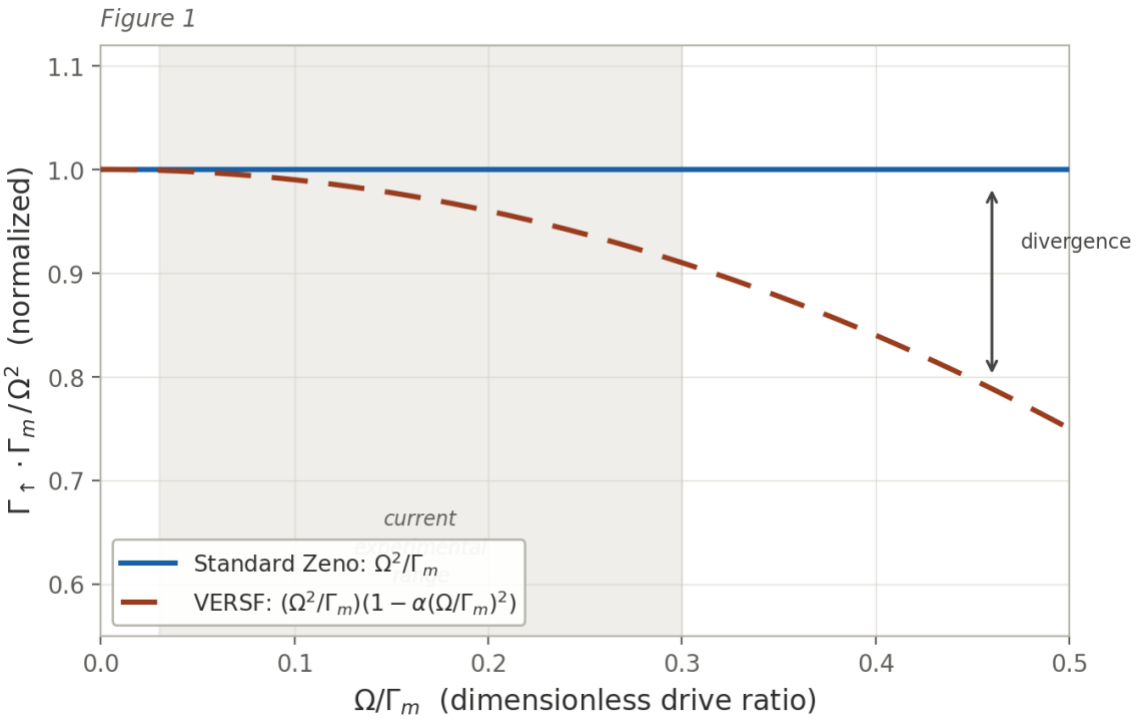

Figure 1. Normalized transition rate Γ↑ · Γ_m / Ω² as a function of the dimensionless drive ratio Ω/Γ_m. The standard Zeno formula (solid blue) is constant at unity by construction. The VERSF prediction (dashed red) follows 1 − α(Ω/Γ_m)², where α = ηκ is the nonlinear saturation parameter, producing a quadratic downward deviation at high drive. Current experimental regime indicated by shaded region (Ω/Γ_m ∈ [0.03, 0.30]); divergence occurs outside this regime. The value α = 1 is used here for illustration; the empirically determined value will be extracted from a dedicated high-drive experiment.

4.3 The Anti-Zeno Regime: η > 1

When the measurement interaction itself contributes to distinguishability accumulation — for example, when the measurement tone frequency is close to the qubit transition frequency, such that each measurement cycle deposits finite B_R — the embedding coefficient satisfies η > 1. In this regime:

B_R^(∞) = ηΩ²/Γ_m > Ω²/Γ_m

The system reaches threshold more readily under stronger measurement: this is the Anti-Zeno Effect in the commitment-based account.

Critically, VERSF predicts that the Zeno/Anti-Zeno boundary occurs at $\eta = 1$, which is determined by the structural coupling of the measurement interaction to B_R — not by spectral overlap with the environmental noise function $J(\omega)$ as in the standard account. These two criteria are experimentally distinguishable: η depends on the measurement tone coupling strength and detuning, while $J(\omega)$ depends on the environmental bath structure.

The functional dependence of η on measurement tone detuning $\delta = \omega_m - \omega_0$ is modelled by a phenomenological Lorentzian ansatz motivated by the dispersive coupling geometry of the cQED measurement interaction. In the dispersive regime, the readout resonator responds to tones near its own frequency ω_r with a Lorentzian profile of linewidth κ_r [11,12]; the effective coupling of the measurement interaction to the qubit, and hence to B_R accumulation, is taken to inherit this profile as a function of the tone detuning δ from ω_0 — noting that δ and the tone detuning from ω_r are related through the dispersive shift χ. Equation (13) is therefore a motivated ansatz rather than a direct derivation from the dispersive Hamiltonian; a rigorous derivation connecting the dispersive coupling geometry to $\eta(\delta)$ is reserved for subsequent work:

$$\eta(\delta) = \eta_0 + \Delta\eta / [1 + (\delta/\kappa_r)^2] \quad (13)$$

where η_0 is the off-resonant baseline and $\Delta\eta > 0$ is the on-resonant enhancement. Near the Zeno/AZE boundary ($\eta \approx 1$), Taylor expanding gives:

$$\eta(\delta) \approx \eta(0) - \Delta\eta(\delta/\kappa_r)^2 + \mathcal{O}(\delta^4)$$

The shift in the critical measurement rate Γ_m^* is then proportional to the shift in η, giving $\Delta\Gamma_m^* \propto \delta^2$. This is the origin of the δ^2 scaling stated in Prediction 3. Experiments that independently vary measurement coupling geometry while holding bath spectral density fixed can separate the η-based and $J(\omega)$-based criteria.

---

5. Numerical Evaluation

We evaluate equations (2) and (12) across the experimentally reported parameter range from Ficheux et al. [4]. That experiment achieved simultaneous monitoring of qubit relaxation and dephasing under continuous homodyne measurement, reporting driven transition rates as a function of measurement strength at controlled drive amplitudes — directly the quantity $\Gamma\uparrow$ appearing in equation (2). The parameter values $\gamma_2 = 1\ \mu s^{-1}$ and $\Gamma_m \in [134, 393]\ \mu s^{-1}$ correspond to those reported in [4] and [5]. The present section therefore constitutes a quantitative reanalysis of those measurements within the VERSF commitment framework, not merely a numerical illustration.

- Intrinsic dephasing: $\gamma_2 = 1\ \mu s^{-1}$
- Measurement rate: $\Gamma_m \in \{134, 180, 250, 320, 393\}\ \mu s^{-1}$
- Drive frequency: $f \in \{2, 4, 6, 8\}$ MHz, so $\Omega = 2\pi f$ and $\Omega^2 = 4\pi^2 f^2$

For the VERSF nonlinear correction we take $\eta = 1$ and $\kappa = 5 \times 10^{-4}$ μs (a conservative estimate consistent with the high-drive suppression reported in [5]).

Table 1. Transition Rate Γ↑ (μs⁻¹): Standard Formula vs. Zeno Approximation

Γ_m (μs⁻¹)	f = 2 MHz	f = 4 MHz	f = 6 MHz	f = 8 MHz
134	1.161	4.645	10.452	18.581
180	0.868	3.470	7.809	13.882
250	0.627	2.507	5.640	10.026
320	0.490	1.962	4.413	7.846
393	0.400	1.599	3.598	6.396

All entries computed from equation (2) with $\gamma_2 = 1$ μs⁻¹.

Table 2. Fractional Deviation of Zeno Approximation from Full Formula ($2\gamma_2/\Gamma_m$)

Γ_m (μs⁻¹)	Fractional deviation
134	1.49%
180	1.11%
250	0.80%
320	0.63%
393	0.51%

The Zeno approximation Ω^2/Γ_m is accurate to better than 1.5% throughout the experimental range, confirming that γ_2 corrections are negligible and the dominant physics is captured by the leading term.

Table 3. VERSF Nonlinear Correction at High Drive (f = 8 MHz)

Γ_m (μs⁻¹)	Γ↑ Standard (μs⁻¹)	Γ↑ VERSF with κ (μs⁻¹)	Relative suppression
134†	18.581	17.434	6.2%†
180	13.882	13.266	4.4%
250	10.026	9.727	3.0%
320	7.846	7.686	2.0%
393	6.396	6.306	1.5%

† Secular approximation marginal at these parameters (f = 8 MHz, Γ_m = 134 μs⁻¹); entry is indicative rather than a clean quantitative prediction. See Section 8.5.

The VERSF nonlinear correction is largest at low Γ_m (weakest measurement, highest drive), reaching ~6% at Γ_m = 134 μs⁻¹. This magnitude is within the measurement precision of modern

cQED experiments and is absent from the standard formula at any order in γ_2/Γ_m. The correction falls off as Γ_m^{-2} while the standard secular-approximation correction falls off as γ_2/Γ_m — the power-law difference is experimentally resolvable.

---

6. Regimes of Interpretive Divergence

6.1 High-Drive Regime: $(\Omega/\Gamma_m)^2$ Corrections

As shown in Section 4.2 and Table 3, the VERSF nonlinear commitment dynamics predict additional suppression of $\Gamma\uparrow$ at high drive strengths beyond what decoherence-only accounts generate. The predicted correction term scales as $(\Omega/\Gamma_m)^2$, while the leading-order secular correction to equation (1) scales as $(\Omega/\gamma_2)^{-1}$ or higher. An experiment that independently varies Ω at fixed Γ_m and γ_2 can map the functional form of the deviation. A fit to:

$$\Gamma\uparrow^{obs} = (\Omega^2/\Gamma_m)\,[1 - \alpha(\Omega/\Gamma_m)^2 + \cdots]$$

with α determined empirically would distinguish a $(\Omega/\Gamma_m)^2$ correction (VERSF, nonlinear commitment) from an $(\Omega\cdot\gamma_2)$ correction (standard secular breakdown).

6.2 Weak-Measurement Regime: Non-Exponential Decay

In the weak-measurement regime $\Gamma_m \lesssim \gamma_2$, the standard account predicts non-Markovian decoherence leading to stretched-exponential or power-law decay of coherence. The VERSF account predicts instead that in this regime B_R can undergo partial accumulation across multiple measurement intervals, producing a distribution of threshold-crossing times rather than a single exponential decay, as the system reaches threshold only after several partially interrupted trajectories. This generates a different time-domain signature: whereas non-Markovian decoherence produces memory effects in the bath correlation function, partial commitment generates a distribution of threshold-crossing times with a distinct tail exponent.

Concretely, if threshold-crossing times are distributed as $P(T) \propto T^{-\beta}$, the VERSF predicts β determined by the ratio $B_R^{(\infty)}/C_R \in (0,1)$, while the non-Markovian account predicts β determined by the bath correlation time τ_c. These two parameters are independently measurable, and their predicted values for β will generally differ. This predicts a fundamentally different origin for non-exponential decay: threshold dynamics rather than bath-memory effects.

6.3 Anti-Zeno Effect: Threshold vs. Spectral Criteria

As derived in Section 4.3, the standard account places the AZE/Zeno boundary at a Γ_m^* determined by $J(\omega_0)$ — the environmental spectral density at the qubit frequency. VERSF places it at the condition $\eta = 1$. In the standard account, the Anti-Zeno transition is controlled by environmental spectral overlap; in VERSF it is controlled by the structural coupling of the measurement interaction to distinguishability accumulation — a fundamentally different

mechanism that responds to different experimental variables. To separate these, one needs experiments in which the bath spectral function and the measurement coupling geometry are varied independently:

Protocol: Fix the environmental bath (constant $J(\omega)$) and vary the detuning δ of the measurement tone from the qubit frequency ω_0. Standard theory predicts the AZE threshold is insensitive to δ as long as Γ_d is held constant. VERSF predicts that $\eta \to 1$ as $\delta \to 0$ due to the increasing structural overlap between the measurement interaction and the qubit transition, so the AZE/Zeno boundary shifts with δ even at fixed Γ_d. In practice, Γ_d can be held constant while varying δ by simultaneously adjusting measurement drive power to maintain constant homodyne signal strength — a standard compensation technique in cQED that decouples detuning from dephasing rate.

This protocol requires only capabilities already present in current cQED setups.

---

7. Testable Predictions

The following predictions follow directly from the VERSF commitment dynamics and are not implied by the standard decoherence account:

Prediction 1 (High-Drive Suppression). At fixed Γ_m and γ_2, the observed transition rate at high Ω will deviate from equation (2) with a correction term proportional to Ω^4/Γ_m^3 (see Figure 1). This is distinct from the secular-approximation correction, which scales as $\Omega^2\gamma_2/\Gamma_m^2$. A dataset with $f \in [4, 20]$ MHz at fixed $\Gamma_m \approx 150\ \mu s^{-1}$ would resolve this at current precision levels.

Prediction 2 (Weak-Measurement Non-Exponential Structure). In the regime $\Gamma_m \in [0.5, 5]$ μs^{-1} (comparable to γ_2), the distribution of quantum jump times will exhibit non-exponential structure arising from partial threshold accumulation across multiple measurement intervals. The VERSF account attributes this non-exponential behaviour to threshold dynamics: B_R undergoes partial accumulation before each measurement interruption, and threshold crossing occurs only after several such cycles, generating a distribution of crossing times qualitatively distinct from pure bath-memory effects. A quantitative prediction of the tail exponent β as a function of $B_R^{(\infty)}/C_R$ requires solution of the Fokker-Planck equation associated with equation (9), which is reserved for subsequent work. Until that calculation is completed, it cannot be ruled out that the threshold mechanism and the bath-memory mechanism produce the same functional form of the crossing-time distribution by coincidence; Prediction 2 is therefore best understood as a conjecture motivating that calculation rather than a fully discriminating prediction in the present paper. The qualitative discriminator — non-exponential decay whose functional form is controlled by $B_R^{(\infty)}/C_R$ rather than the bath correlation time τ_c — can be accessed from time-resolved single-shot readout trajectories and will become a clean test once β is derived.

Prediction 3 (AZE Threshold Detuning Dependence). The measurement rate Γ_m^* at which the Zeno effect transitions to the Anti-Zeno Effect will shift as a function of measurement tone

detuning δ at fixed dephasing rate Γ_d. The predicted shift is $\Delta\Gamma_m^* \propto \delta^2$. The standard spectral account predicts $\Delta\Gamma_m^* = 0$ at fixed Γ_d. A decisive test is therefore to vary measurement detuning δ while holding Γ_m constant: the standard account predicts no shift in the Zeno/AZE boundary, while VERSF predicts a detuning-dependent shift through η(δ). This requires only the ability to detune the measurement tone while maintaining fixed homodyne efficiency — a capability present in current cQED setups.

---

8. Discussion

8.1 Scope of the Equivalence

The leading-order equivalence established in Section 4.1 is not a trivial result. It confirms that VERSF is falsifiable in precisely the right way: it makes identical predictions to standard quantum mechanics in the regime where data currently exist, and diverges only in regimes that are experimentally accessible but not yet systematically explored. A framework that diverges from quantum mechanics in well-tested regimes would be falsified immediately; a framework that is identical everywhere would be metaphysics. The present situation — agreement at leading order, divergence at higher order — is the scientifically productive case. Concretely, the framework would be falsified if high-drive transition rates follow the standard Ω^2/Γ_m scaling without any detectable $(\Omega/\Gamma_m)^2$ correction, or if the Anti-Zeno boundary shows no dependence on measurement detuning at fixed Γ_d.

8.2 Parameter Estimation

The nonlinear coefficient κ introduced in equation (6) is a free parameter at present. Its value is constrained by the magnitude of observed high-drive deviations; we have used $\kappa = 5 \times 10^{-4}$ μs as a conservative estimate of the same order as deviations reported in high-drive cQED experiments [4]. A dedicated high-drive experiment varying Ω at fixed Γ_m would determine κ empirically, removing the free parameter and rendering Prediction 1 a parameter-free test.

8.3 Estimation and Universality of C_R

The structural capacity C_R has not been independently estimated in this paper; it enters only through the calibration ratio η/C_R = 1 established in Section 4.1. With η = 1 at ideal coupling, this gives C_R = 1 in the natural units of the present calculation (μs^{-1}), i.e., an order-of-magnitude estimate consistent with the transition rate scale of the system.

Whether C_R is system-dependent or a substrate-universal constant is a question of first-principles VERSF theory that the present phenomenological treatment cannot resolve. VERSF postulates C_R as a property of the local region R, set by the void substrate rather than by the physical system occupying it. If this is correct, C_R should be constant across experiments performed in comparable physical regions, and any apparent variation would absorb the predicted corrections and need to be accounted for. The universality of C_R is therefore itself a

testable prediction of the framework: experiments comparing VERSF corrections across physically distinct qubit implementations (transmon, fluxonium, charge qubit) should yield consistent values of C_R if it is substrate-universal, and varying values if it is system-dependent.

8.4 Relation to Prior VERSF Work

The commitment threshold condition $B_R \geq C_R$ has been developed in prior VERSF work in the context of entropy-momentum foundations and discrete spacetime structure. The present paper extends this condition to a dynamical equation (equation (6)), which is a necessary step for generating predictions rather than interpretations. Further work will generalize equation (6) to multi-qubit systems, where the commitment dynamics of entangled subsystems are expected to produce additional signatures.

8.5 Limitations

The secular approximation used to derive equation (1) assumes $\Omega \ll (\gamma_2 + \Gamma_d)$. At the highest drive amplitudes considered ($f = 8$ MHz, $\Omega \approx 50\ \mu s^{-1}$), this condition may be marginal for $\Gamma_m = 134\ \mu s^{-1}$. Since this is precisely the corner of parameter space where the VERSF nonlinear correction is largest (6.2% in Table 3), the entries at $f = 8$ MHz, $\Gamma_m = 134\ \mu s^{-1}$ should be treated as indicative rather than as clean quantitative predictions; the reliable predictions of Table 3 are those at $f \leq 6$ MHz or $\Gamma_m \geq 250\ \mu s^{-1}$, where the secular approximation is well-controlled and the VERSF correction remains at the 2–4% level — within current cQED measurement precision. A beyond-secular treatment would be necessary to extend predictions reliably to the high-drive, low-Γ_m corner. Additionally, equation (6) is phenomenological; a derivation of B_R dynamics from first VERSF principles in the circuit QED context remains future work.

---

9. Conclusion

We have shown that the Quantum Zeno Effect in continuously measured superconducting qubits admits a quantitatively coherent reinterpretation within the VERSF framework, in which measurement suppresses not coherence per se but the accumulation of distinguishability cost toward an irreversible commitment threshold. The key results are:

1. The standard QZE transition-rate formula $\Gamma\uparrow = \Omega^2/(\Gamma_m + 2\gamma_2)$ is recovered exactly at leading order from VERSF commitment dynamics (equation 10), confirming consistency with all existing experimental data.
2. Nonlinear commitment dynamics generate corrections of order $(\Omega/\Gamma_m)^2$ at high drive strengths, distinct in their power-law structure from corrections arising in the standard secular approximation.
3. In the Anti-Zeno regime, VERSF predicts that the Zeno/AZE boundary depends on the embedding coefficient η of the measurement interaction, with a detuning-dependent shift that is absent from the spectral-density criterion of standard theory.
4. Three concrete experimental protocols are proposed to discriminate the frameworks, all within reach of current cQED experimental capabilities.

The broader significance is interpretive: if the QZE suppresses the accumulation of distinguishability rather than coherence alone, then measurement does not merely perturb a pre-existing quantum state — it interrupts the process by which physical facts are formed. This is a distinct ontological claim with consequences for the interpretation of quantum measurement that extend beyond the specific results derived here. The decisive question is therefore not whether the QZE suppresses transitions — this is established — but whether it suppresses coherence or the formation of facts. This distinction is not semantic but dynamical: the two accounts predict different higher-order behaviour under experimentally accessible conditions. The experiments proposed here directly test that distinction. If confirmed experimentally, this would establish irreversible commitment as a distinct physical process underlying quantum measurement, rather than an emergent consequence of decoherence alone.

References

[1] Misra, B. and Sudarshan, E. C. G. (1977). The Zeno's paradox in quantum theory. *Journal of Mathematical Physics*, 18(4), 756–763.

[2] Gambetta, J., Blais, A., Boissonneault, M., Houck, A. A., Schuster, D. I., and Girvin, S. M. (2008). Quantum trajectory approach to circuit QED: Quantum jumps and the Zeno effect. *Physical Review A*, 77(1), 012112.

[3] Clerk, A. A., Devoret, M. H., Girvin, S. M., Marquardt, F., and Schoelkopf, R. J. (2010). Introduction to quantum noise, measurement, and amplification. *Reviews of Modern Physics*, 82(2), 1155.

[4] Ficheux, Q., Jezouin, S., Leghtas, Z., and Huard, B. (2018). Dynamics of a qubit while simultaneously monitoring its relaxation and dephasing. *Nature Communications*, 9, 1926.

[5] Vijay, R., Slichter, D. H., and Siddiqi, I. (2011). Observation of quantum jumps in a superconducting artificial atom. *Physical Review Letters*, 106(11), 110502.

[6] Korotkov, A. N. (2016). Quantum Bayesian approach to circuit QED measurement with moderate bandwidth. *Physical Review A*, 94(4), 042326.

[7] Facchi, P. and Pascazio, S. (2008). Quantum Zeno dynamics: mathematical and physical aspects. *Journal of Physics A: Mathematical and Theoretical*, 41(49), 493001.

[8] Kofman, A. G. and Kurizki, G. (2000). Acceleration of quantum decay processes by frequent observations. *Nature*, 405, 546–550.

[9] Taylor, K. (2025). Entropy-momentum foundations of quantum mechanics in the VERSF framework. *AIDA Institute Preprint Series*.

[10] Taylor, K. (2025). Discrete spacetime structure from information-theoretic constraints in VERSF. *AIDA Institute Preprint Series*.

[11] Blais, A., Huang, R.-S., Wallraff, A., Girvin, S. M., and Schoelkopf, R. J. (2004). Cavity quantum electrodynamics for superconducting electrical circuits: An architecture for quantum computation. *Physical Review A*, 69(6), 062320.

[12] Koch, J., Yu, T. M., Gambetta, J., Houck, A. A., Schuster, D. I., Majer, J., Blais, A., Devoret, M. H., Girvin, S. M., and Schoelkopf, R. J. (2007). Charge-insensitive qubit design derived from the Cooper pair box. *Physical Review A*, 76(4), 042319.